Published on 13 March 2014. Downloaded by Changchun Institute of Optics, Fine Mechanics and Physics, CAS on 26/03/2015 01:05:15.

JAAS

PAPER

View Article Online
View Journal | View Issue

Effect of sample position on collinear femtosecond double-pulse laser-induced breakdown spectroscopy of silicon in air

Cite this: *J. Anal. At. Spectrom.*, 2014, **29**, 1105

Hongxia Qi,[a] Suyu Li,[a] Ying Qi,[a] Anmin Chen,*[ab] Zhan Hu,*[a] Xuri Huang,[b] Mingxing Jin[ac] and Dajun Ding[a]

A femtosecond double-pulse laser was used to induce the plasma of silicon in air. The laser wavelength was 800 nm. The interpulse delay of the femtosecond double-pulse was from −20 ps to 100 ps. During the experiment, the spectral line was fixed at the wavelength of 288.157 nm. The emission intensity was observed to lead to a significant increase by choosing the proper sample position. The range of the sample position is from 5.17 mm to 5.27 mm. And, the best sample position for the higher laser fluence was different from the position for the lower laser fluence. At the higher laser fluence, the optimized emission intensity can be obtained at either side of the best focal position for all interpulse delays of the double-pulse. The phenomena can be explained by the nonlinear propagation of the femtosecond laser pulse in air. At the lower laser fluence, the best sample position will change from one side to both sides with the increase of the interpulse delay of the double-pulse. The results showed that the effect of the sample position can be especially advantageous in the context of femtosecond double-pulse laser-induced breakdown spectroscopy. The study will lead a further improvement in the applications of the femtosecond double-pulse laser.

Received 7th January 2014
Accepted 13th March 2014

DOI: 10.1039/c4ja00006d

www.rsc.org/jaas

1 Introduction

Laser-induced breakdown spectroscopy (LIBS) is a popular technique involving laser ablation of a sample and analysis of the optical emission from the laser-generated plasma to determine the elements within the sample.[1] LIBS has already been applied in a wide range of applications, such as civilian and military environmental monitoring, cultural heritage analysis and characterization, and biological and medical identification, as well as space exploration.[2–5] In recent years, many new experimental methods have been used to improve the sensitivity of LIBS, such as plasma confinement,[6–8] fast spark discharge,[9,10] magnetic field,[11–13] double-pulse,[14–17] and so on.

With the development of a variety of laser technologies, a femtosecond laser was introduced into laser ablation. The interaction of the femtosecond laser and the material provided some special features to the ablation process as a lower damage threshold and a higher efficiency, which are different for the nanosecond laser. The other advantages included the small heat affected zone, better depth resolution, and faster broadband background decay. By comparing single-shot LIBS with femtosecond and nanosecond laser pulses, the femtosecond spectrum was well-resolved and presented a very low background emission, allowing signal accumulation for a large number of pulses. And, plasma emission was found to vary much more rapidly with time than in the case of the nanosecond laser produced plasma. Due to the advantage of the nanosecond double-pulse laser in LIBS, the femtosecond double-pulse configuration has been used for the studies of LIBS. The double-pulse technique can be carried out in two different pulse configurations called orthogonal[18,19] and collinear,[20,21] referring to the relative directions of the two laser pulses. In both configurations the laser is fired twice with pulse separation.[22] The interpulse delay of two pulses was controlled by the precise stepper motor stage. The range of the interpulse delay was from 0 ps to hundreds of ps. Compared with the results induced by the femtosecond single-pulse laser, increasing or decreasing the interpulse delay of the femtosecond double-pulse, some new results generated by the femtosecond double-pulse laser can be obtained. For example, enhancement of plasma emission,[23] reducing nanoparticles,[24] plume composition control,[25,26] and so on. In particular, at the same whole laser energy, the femtosecond double-pulse technique in LIBS can provide the higher luminosity of plasma in comparison with the femtosecond single-pulse and thus efficiently improve the accuracy of the measurements.[27–30] Furthermore, some theoretical research has been also carried

[a]*Institute of Atomic and Molecular Physics, Jilin University, Changchun 130012, China. E-mail: amchen@jlu.edu.cn; huzhan@jlu.edu.cn*

[b]*Institute of Theoretical Chemistry, State Key Laboratory of Theoretical and Computational Chemistry, Jilin University, Changchun 130012, China*

[c]*State Key Laboratory of Laser Interaction with Matter, Changchun Institute of Optics, Fine Mechanics and Physics, Chinese Academy of Sciences, Changchun 130033, China*

Published on 13 March 2014. Downloaded by Changchun Institute of Optics, Fine Mechanics and Physics, CAS on 26/03/2015 01:05:15.

out. The phase change mechanisms were studied during femtosecond laser pulse train ablation of nickel thin films by the method of molecular dynamics simulation.[31] The femtosecond pulse train laser heating metal film demonstrated the effects of repetition rate and pulse separation on the ablation.[32,33] The temporal and spatial variations in the optical properties were investigated for pulse train laser heating.[34] The emission enhancement on the plasma from a copper surface under the double-pulse femtosecond laser is studied by means of a 1D two-temperature equation and the Boltzmann equation.[35] These studies investigated the effect of laser energy and pulse separation on the femtosecond double-pulse LIBS. But, many reports indicated that the LIBS may vary with the various laser parameters, including laser wavelength, pulse width, intensity, and so on.[36–39] The properties of LIBS also depend on the spot size, as well as the sample position with respect to the distance between the target and the lens. The sample position can influence the expansion process of the plasma plume due to the interaction of the plasma plume and the changed laser spatial energy distribution.[36,40] The relationship between the conversion efficiency of the extreme-ultraviolet emission and the spot size was also studied by changing the lens-to-samples distance, and a double hump structure was observed during scanning of the target lens.[37] Until now almost no studies focused on studying the effect of the sample position on the LIBS signal using the femtosecond double-pulse laser.

In this paper, the emission enhancement on the plasma from a silicon surface under the collinear double-pulse femtosecond laser was studied by moving the sample position. The emission signal enhancement was observed in the double-pulse interpulse delay range from −20 ps to 100 ps. Our results showed that the sample position is found to be important for obtaining the optimal femtosecond double-pulse laser-induced breakdown spectroscopy. The study will lead a further improvement to the applications of the double-pulse LIBS.

2 Experimental details

The schematic diagram of the standard pump-probe experimental setup is shown in Fig. 1. The laser system is a regenerative amplified Ti:sapphire laser (Spectra Physics Tsunami oscillator and Spitfire amplifier). The full-width at half maximum (FWHM) is 100 fs, the output maximum energy is about 300 μJ, the wavelength is 800 nm, and the repetition rate is 1 kHz. The delivered single laser pulse is produced by the computer-triggered Pockel cell of the amplifier. The individual pulse is splitted into two sub-pulses using a Michelson interferometer. The interpulse delay may be changed from −30 ps to 110 ps. By the combination of a Glan laser polarizer and a half-wave plate, the whole energy of each pulse can be attenuated to the desired value. The subpulses are directed using a beam splitter into a microscope objective (10×, NA = 0.25), which focuses them onto the target material with a focal diameter of 7.2 μm. We use a knife edge to measure the beam profile. The silicon target is mounted on a computer-controlled *X*–*Y*–*Z* stage, which guarantees that the sample location is new before each laser shot (*X*–*Y*). The sample Si is positioned with its normal axis

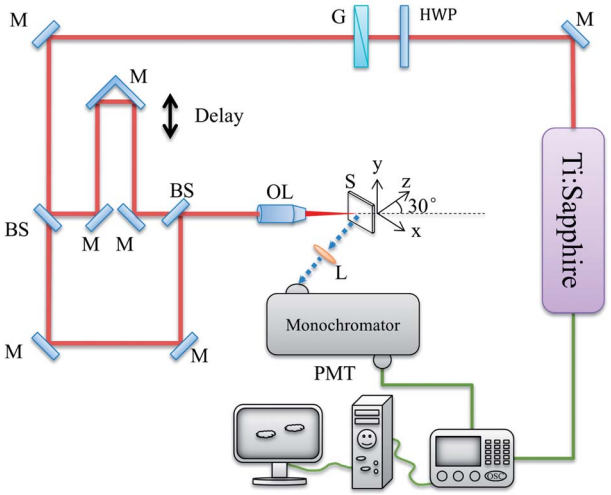

Fig. 1 The schematic drawing of the apparatus. Components include beam splitter (BS), mirror (M), lens (L), glan laser polarizer (G), half-wave plate (HWP), objective lens (OL), sample (S), and photomultiplier tube (PMT).

at an angle of 30° with respect to the laser beam direction. So, there is an angle of 30° between the *Z* direction and the laser incident direction. All experiments are performed in air at atmospheric pressure. The each data point is an average of typically 20 shots. In the experiment, both pump pulses are s-polarized. The plasma emission perpendicular to the laser beam is collected by an *f*/2.0 lens, focused into a 0.25 m monochromator, and detected with a photomultiplier tube (PMT (Hamamatsu, R456)). The voltage of PMT is 1 kV.

3 Results and discussion

In this experiment, we investigated the position of the focal point and the diameter of the gaussian beam by the knife-edge method.[41] The energy was 3.8 μJ and 56.8 μJ, respectively. The selected emission line was the Si(I) at 288.157 nm, produced by the $3s^2 2p^2\ (1D_2) \leftarrow 3s^2 2p4s\ (1P_1)$ transition. In order to determine the location of the grating of this monochromator, the grating was rotated using a stepper motor. Using the oscilloscope and the computer, we could obtain the detected

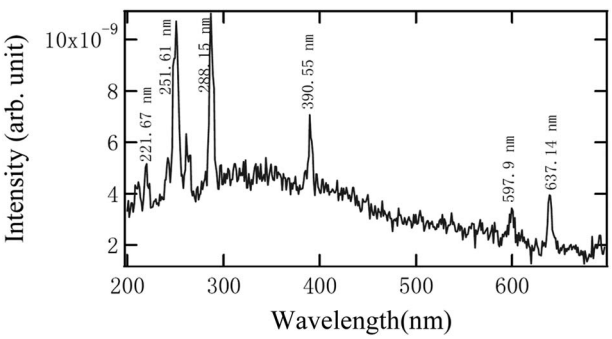

Fig. 2 The recorder spectroscopy of Si plasma by rotating the grating. The laser fluence is 4.65 J cm^{-2}.

This journal is © The Royal Society of Chemistry 2014

Published on 13 March 2014. Downloaded by Changchun Institute of Optics, Fine Mechanics and Physics, CAS on 26/03/2015 01:05:15.

spectroscopy of the PMT. The range of the measured spectroscopy was 200–700 nm. Fig. 2 shows the plot of the emission spectroscopy of femtosecond laser-induced Si plasma. The laser fluence is 4.65 J cm^{-2}. And, we recorded the corresponding relationship between the location of the stepper motor and the wavelength. By this method, the location of the grating was fixed at the wavelength of 288.157 nm.

The spectroscopy emitted from the plasma can be enhanced by changing the interpulse delay of the femtosecond double-pulse. And, the spectroscopy of the plasma is strongly dependent on the laser energy and the target properties. The distribution of the emission intensity was obtained by moving the time delay stepper motor and the *Z*-axis of the three-dimensional stage with the sample. The distribution of the emission intensity produced by femtosecond double-pulse laser-induced spectroscopy with the different sample position and the interpulse delay after the onset of plasma are given in Fig. 3 and 4. The whole laser fluence was 9.29 J cm^{-2} and 139.63 J cm^{-2}, respectively. The energy of each sub-pulse was 4.65 J cm^{-2} and 69.82 J cm^{-2}, respectively. The measured position of the focal point was $Z = 5.21$ mm. When Z was greater than the position of the focal point, the focal point was on the outside of the sample. The emission intensity was the integration of the whole plasma spectroscopy decay at the wavelength of 288.157 nm. It was observed (Fig. 3 and 4) that at a relatively high laser fluence (139.63 J cm^{-2} in Fig. 4), the emission intensity was higher than the low laser fluence (9.29 J cm^{-2} in Fig. 3), and the decay time of plasma was longer observed from the oscilloscope. Since the high laser energy caused the plasma brighter and its luminosity lasted for a longer period of time.[42,43] The emission intensity was enhanced by changing the interpulse delay of the femtosecond double-pulse. The mechanism of the plasma emission enhancement: it was possible that the emission intensity

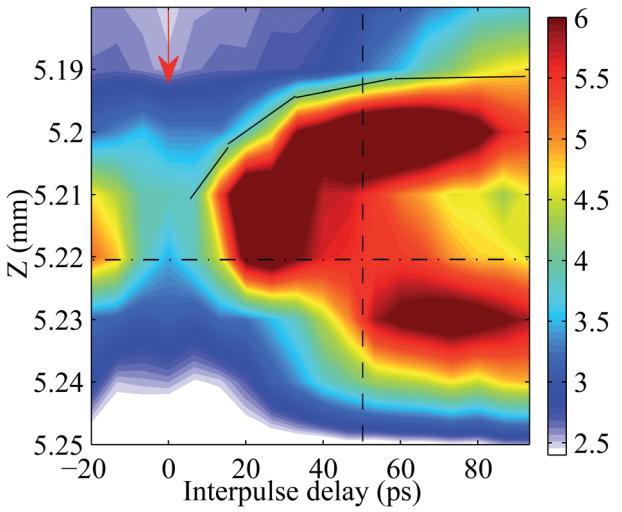

Fig. 3 The distribution of the emission intensity with the interpulse delay of the double-pulse and the position of the sample. The arrow is the direction of the laser. The evolution of the focal point is from the sample inside to outside. The laser fluence is 9.29 J cm^{-2}. The fluence of each sub-pulse is 4.65 J cm^{-2}. The recorded wavelength is 288.157 nm.

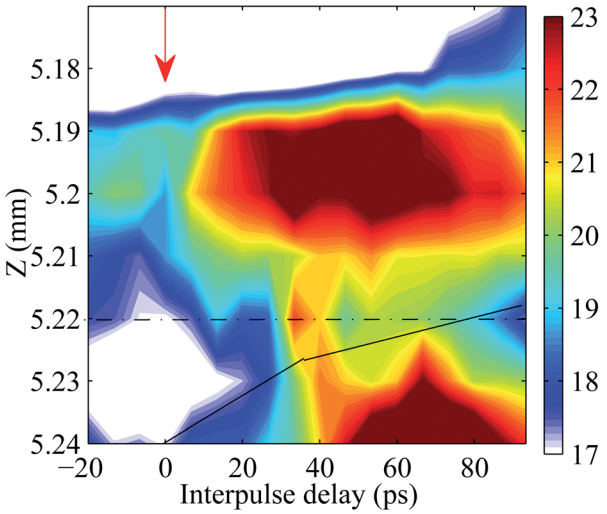

Fig. 4 The distribution of the emission intensity with the interpulse delay of the double-pulse and the position of the sample. The arrow is the direction of the laser. The evolution of the focal point is from the sample inside to outside. The laser fluence is 139.63 J cm^{-2}. The fluence of each sub-pulse is 69.82 J cm^{-2}. The recorded wavelength is 288.157 nm.

increased because more material was ablated from the target surface by the femtosecond double-pulse laser as the result of the surface transformation excited by the first pulse; the enhanced effect may be due to the plasma reheating of the second pulse; the hydrodynamic effect produced by the first pulse may change the propagation of the laser pulse and the expansion of the plasma plume generated by the second pulse.[15,29,30,44–47]

For the different sample position, the plasma emission intensity firstly began to rise with the interpulse delay, and then dropped. At the interpulse delay of the zero point, the emission intensity was weak compared with the other interpulse delay of double-pulse (Fig. 3 and 4). Fig. 5 shows the emission intensity selected from Fig. 3 with the interpulse delay of the double-pulse at the different position of the sample. The positions are $Z = 5.19$ mm, $Z = 5.20$ mm, $Z = 5.23$ mm, and $Z = 5.24$ mm, respectively. As seen from this plot, the enhancement of the emission intensity was sensitive to the interpulse delay of the double-pulse. We noticed that two main changing regions in Fig. 5(a) were distinguished including the increased region and the decreased region. However, in Fig. 5(b), the emission intensity monotonically increased with the interpulse delay of the double-pulse. The difference between Fig. 5(a) and (b) is the position of the sample. In the case of the different sample position, the sample position can obviously affect the evolution of the emission intensity with the interpulse delay of the double-pulse. So, the emission intensity of the plasma generated by the femtosecond double-pulse laser should be further discussed.

In order to understand the problem about the effect of the sample position, the emission intensity selected from Fig. 3 with the position of the sample at the different interpulse delay of the double-pulse is shown in Fig. 6. As seen from Fig. 6(a), it

Published on 13 March 2014. Downloaded by Changchun Institute of Optics, Fine Mechanics and Physics, CAS on 26/03/2015 01:05:15.

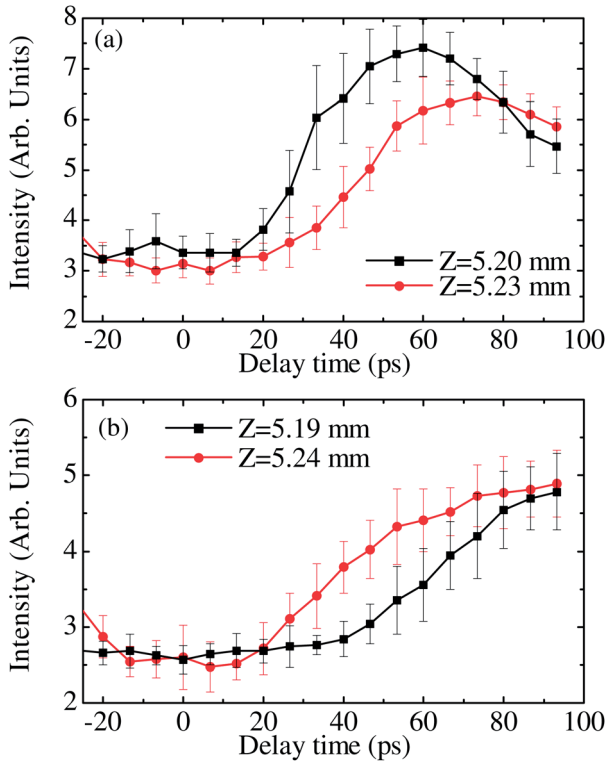

Fig. 5 The emission intensity from Fig. 3 with the interpulse delay of the double-pulse at the different position of the sample. The position (Z): (a) 5.20 mm, and 5.23 mm; (b) 5.19 mm, Z = 5.24 mm. The laser fluence is 9.29 J cm^{-2}. The fluence of each sub-pulse is 4.65 J cm^{-2}. The recorded wavelength is 288.157 nm.

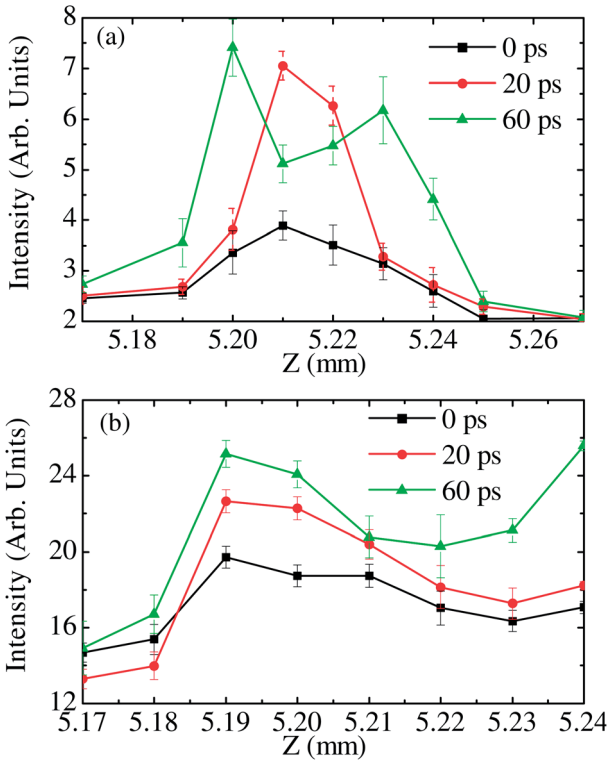

Fig. 6 The emission intensity from Fig. 3 and 4 with the position of the sample at the different interpulse delay of the double-pulse. The interpulse delay is 0 ps, 20 ps, and 60 ps, respectively. The whole laser fluence is 9.29 J cm^{-2} (a) and 139.63 J cm^{-2} (b), respectively. The recorded wavelength is 288.157 nm.

was interesting to notice that the emission intensity for the interpulse delay of 60 ps showed a dip at the best focal position (Z = 5.21 mm) compared with the emission for the interpulse delay of 0 ps and 20 ps. Hence, the optimized emission intensity can further be obtained at either side of the best focal position with the increase of the interpulse delay (this phenomenon can also be observed in Fig. 3). This revealed that the emission intensity was slightly away from the best focal position at the interpulse delay of 60 ps, where the emission was nearly 50% higher than at the best sample position. However, in Fig. 6(b), the higher laser energy was used in the experiment. The result showed that the sample-lens scan effect on the emission intensity was not almost dependent on the interpulse delay of the double-pulse. For the different interpulse delay, the trend of the intensity was the same with the change in the sample position. A similar dip had also been noticed in the vicinity of the best focal position. The focal position is not the best condition for obtaining the higher plasma emission. These results showed that the emission intensity will not only be related to the condition of the laser source (such as: delay, laser energy, laser wavelength, and so on) and the signal detection system but also be related to the sample position.

In femtosecond single-pulse laser ablation, for metals, the absorption mechanism is the inverse bremsstrahlung (IB) absorption process.[48] However, for semiconductors (silicon), the energy of the laser pulse is first absorbed by the valence band electrons through inter-band absorption because of the lack of free electrons.[43] So, different from the metals, the single-photon or multi-photon (MP) absorption is important for femtosecond irradiation of silicon.[43,49,50] The electrons excited into the valence band will absorb more energy of the laser pulse by the IB absorption process, similar to the cases in the metals. The absorbed laser energy of the sample can be divided into two parts: the thermal energy of the electrons and the energy consumed to overcome the band gap.[49] For the femtosecond double-pulse laser, the absorption mechanism of the second pulse is the major IB process. Because, a large number of free electrons have been generated by the first pulse.[49] The absorption efficiency of IB is much higher than the absorption efficiency of MP.[51] So, the second pulse is crucial for the enhancement of the plasma emission based on the plasma reheating mechanism.

In Fig. 3 and 4, the emission intensity can be obviously divided into two higher regions. For the higher laser fluence of 139.63 J cm^{-2} (Fig. 4), two higher emission regions were observed with the sample position in the beginning. Since, the whole experiment was carried out in air. The nonlinear pulse propagation problems of the femtosecond laser should be considered, many researchers had directly seen the self-focusing or self-defocusing effect by using laser pulse propagation through a transparent medium.[52–57] These changes in the spatial energy distribution of the laser beam can be caused by

This journal is © The Royal Society of Chemistry 2014

Published on 13 March 2014. Downloaded by Changchun Institute of Optics, Fine Mechanics and Physics, CAS on 26/03/2015 01:05:15.

nonlinear effects resulting from the femtosecond laser beam.[58] Hence, the focal length would become shorter due to the self-focusing effect. It indicated that the redistribution of laser spatial energy would change the emission of plasma spectroscopy induced by the plasma reheating of the second femtosecond pulse laser.[59] The laser intensity of the second pulse was important for the plasma reheating. The higher laser intensity will lead to stronger plasma emission. The self-focusing or self-defocusing effect will influence the laser intensity along the laser incident direction. That was the *Z*-axis direction of the stage.

Based on the nonlinear propagation theory of a femtosecond optical pulse, for the first femtosecond pulse (or single pulse), the index of refraction was expressed as[60]

$$n = n_0 + n_2 I - \Delta n_1 \quad (1)$$

where n_0 is the linear index of refraction in air, $n_2 I$ is the Kerr nonlinear index of refraction, n_2 and I are the coefficient of the Kerr nonlinear index of refraction and the laser intensity, respectively. The item of the defocusing is $\Delta n_1 = 4\pi e^2 N_{1e}(t)/2m_e\omega_0{}^2$, N_{1e} was the time dependent electron density generated by first pulse, e and m_e were the electronic charge and mass, respectively, and ω_0 was the frequency of the laser pulse. For the second femtosecond pulse, the energy was equal to the energy of the first pulse, and the index of refraction considered the electron intensity of the first pulse (Δn_1) was expressed as

$$n = n_0 + n_2 I - \Delta n_2 - \Delta n_1 \quad (2)$$

where $\Delta n_2 = 4\pi e^2 N_{2e}(t)/2m_e\omega_0{}^2$ and N_{2e} is the electron density of the second pulse. The contours (Fig. 3 and 4) clearly showed that the higher emission of the plasma moved opposite to the laser incident direction. And, the plasma emission produced by the femtosecond self-focusing or self-defocusing effect in air is observed in Fig. 4 and 6(b). In this case, the focal position was in the self-defocusing.

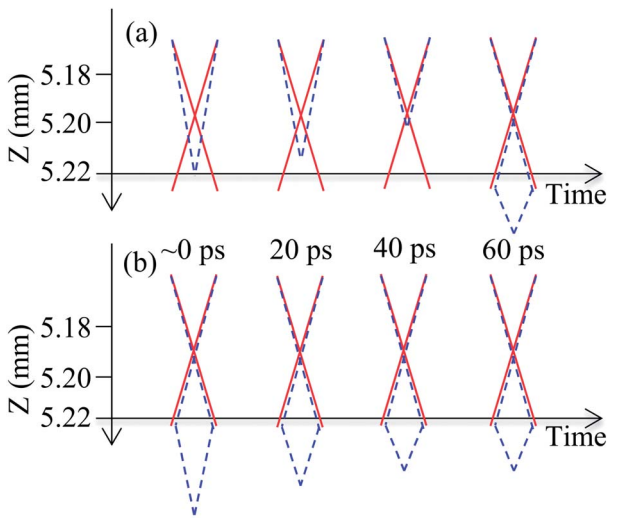

Fig. 7 Schematic diagram of the spatial distribution for the femtosecond laser at the different interpulse delay in air: (a) lower laser fluence (9.29 J cm^{-2}), (b) higher laser fluence (139.63 J cm^{-2}). The solid line is the focusing situation of the first pulse; the dashed line is the focusing situation of the second pulse. The horizontal axis is the normal geometric focal position (Z = 5.22 mm).

For the lower laser fluence (9.29 J cm^{-2}), in Fig. 3, there were not two higher regions at the shorter interpulse delay index. The refocusing effect of the second pulse cannot take place due to the larger defocusing of Δn_1 and Δn_2. The range was 0 ps to 50 ps. When the interpulse delay was greater than 50 ps, two higher emission intensity regions may be observed. The evolution schematic diagram of the focusing position was shown in Fig. 7(a). At the interpulse delay of near 0 ps, the focus position of the first femtosecond pulse was in the front of the focal position based on the large Kerr nonlinear effect. The focused position of the second pulse just was at the original focal position based on the large electron intensity (small index of refraction). Since, the first femtosecond pulse excited the air and generated a large number of electrons.[51] At this time, electron density was maximum. According to eqn (2), the electron density was the sum of the electron density produced by the first pulse and the second pulse. The index of refraction was minimum. The second femtosecond pulse focused at the focal position. At this position, the laser intensity of the second pulse was maximum, the effect of plasma reheating was the best, and the intensity of plasma emission was the highest. With the increase of the interpulse delay of the double-pulse, the electron density decreased,[51,61] the index of refraction increased, and the focused position of the second femtosecond pulse moved opposite to the laser incident direction. Until the focused position of the second pulse infinitely close to the focal point of the first pulse. The intensity of plasma emission on the sample position of the *Z*-axis varied according to the focused position of the second pulse. At this moment (about 50–60 ps), the refocusing effect can be observed (Fig. 3). Because, for the second pulse, the item of the nonlinear Kerr effect ($n_2 I$) was greater than the item of the defocusing (Δn_1 and Δn_2). At this lower laser fluence (9.29 J cm^{-2}), for the interpulse delay of 50–60 ps, the electron density produced by the first pulse decayed to a lower value at the first focused position, the absorption of this ionization region for the second pulse can be ignored, and the transmitted laser energy obviously increased compared with the shorter interpulse delay.[62,63] In this case, the refocusing effect of the second pulse can take place by the transmitted laser energy. And, the second focused point will appear. So, in the range of 50–90 ps, two focused points appeared at the laser direction (*Z*-axis). In other words, the second pulse had two high laser intensities along the moved position of the sample. Two higher emission regions along the laser direction can be observed.

However, in Fig. 4, at the beginning (Fig. 6(b)), the enhanced plasma emission produced by the focusing and refocusing effect can be observed. For the higher laser fluence (139.63 J cm^{-2}), when the interpulse delay is near 0 ps, although the electron density produced by the first pulse was very high at the first focused position, the transmitted laser energy of the second pulse was large enough to generate the refocusing effect (the second focused point appeared) due to the strong nonlinear Kerr effect. Two higher emission regions can be

Published on 13 March 2014. Downloaded by Changchun Institute of Optics, Fine Mechanics and Physics, CAS on 26/03/2015 01:05:15.

observed. With the increase of the time, the electron density decreased at the first focused position, the transmitted laser energy gradually increased. The nonlinear Kerr effect became stronger. The index of refraction also became larger. The position of the refocusing obviously moved opposite to the laser incident direction at the second focused point. The distance between the focusing (the first focused position) and the refocusing (the second focused position) decreased with the increase of the interpulse delay of the double-pulse. The schematic diagram is shown in Fig. 7(b). This provided a better understanding about the effect of sample position in femtosecond double-pulse LIBS, leading to better conditions for femtosecond double-pulse LIBS production.

4 Conclusion

In conclusion, the enhancement of plasma emission was demonstrated by the femtosecond double-pulse laser-induced silicon plasma in air. The enhancement may be further increased by recording the dependence of emission intensity on the sample position. For the higher laser fluence, the optimized emission intensity can be obtained at either side of the best focal position for all interpulse delays of the double-pulse. For the lower laser fluence, the best sample position will change from one side to both sides with the increase of the interpulse delay of the double-pulse. The observed phenomena can be explained by the nonlinear propagation of the femtosecond laser pulse in air. The results may also be used to understand the better way to optimize femtosecond double-pulse LIBS.

Acknowledgements

This project was supported by the Fundamental Research Funds for the Central Universities in China, the Research Fund for the Doctoral Program of Higher Education in China (Grant no. 20130061110021), the National Basic Research Program of China (973 Program, grant no. 2013CB922200), and the National Natural Science Foundation of China (grant nos 10974069, 11374124, and 11034003).

References

1 L. J. Radziemski and D. A. Cremers, *Laser-induced plasmas and applications*, CRC Press, 1989, vol. 21.
2 K. Y. Yamamoto, D. A. Cremers, M. J. Ferris and L. E. Foster, *Appl. Spectrosc.*, 1996, **50**, 222–233.
3 G. Arca, A. Ciucci, V. Palleschi, S. Rastelli and E. Tognoni, *Appl. Spectrosc.*, 1997, **51**, 1102–1105.
4 M. Baudelet, L. Guyon, J. Yu, J.-P. Wolf, T. Amodeo, E. Fréjafon and P. Laloi, *J. Appl. Phys.*, 2006, **99**, 084701.
5 B. Sallé, D. A. Cremers, S. Maurice and R. C. Wiens, *Spectrochim. Acta, Part B*, 2005, **60**, 479–490.
6 Z. Hou, Z. Wang, J. Liu, W. Ni and Z. Li, *Opt. Express*, 2013, **21**, 15974–15979.
7 Z. Wang, Z. Hou, S.-l. Lui, D. Jiang, J. Liu and Z. Li, *Opt. Express*, 2012, **20**, A1011–A1018.
8 A. M. Popov, F. Colao and R. Fantoni, *J. Anal. At. Spectrom.*, 2010, **25**, 837–848.
9 W. Zhou, X. Su, H. Qian, K. Li, X. Li, Y. Yu and Z. Ren, *J. Anal. At. Spectrom.*, 2013, **28**, 702–710.
10 K. Li, W. Zhou, Q. Shen, Z. Ren and B. Peng, *J. Anal. At. Spectrom.*, 2010, **25**, 1475–1481.
11 P. K. Pandey and R. K. Thareja, *Phys. Plasmas*, 2013, **20**, 022117.
12 S. Harilal, M. Tillack, B. Oshay, C. Bindhu and F. Najmabadi, *Phys. Rev. E: Stat., Nonlinear, Soft Matter Phys.*, 2004, **69**, 026413.
13 C. Pagano and J. Lunney, *J. Phys. D: Appl. Phys.*, 2010, **43**, 305202.
14 X. Mao, X. Zeng, S.-B. Wen and R. E. Russo, *Spectrochim. Acta, Part B*, 2005, **60**, 960–967.
15 K. Rifai, S. Laville, F. Vidal, M. Sabsabi and M. Chaker, *J. Anal. At. Spectrom.*, 2012, **27**, 276–283.
16 L. Guo, B. Zhang, X. He, C. Li, Y. Zhou, T. Wu, J. Park, X. Zeng and Y. Lu, *Opt. Express*, 2012, **20**, 1436–1443.
17 H. Sobral, C. Sánchez-Aké, R. Sanginés, E. Alvarez-Zauco and K. Jiménez-Durán, *J. Phys. D: Appl. Phys.*, 2011, **44**, 085201.
18 I. Choi, X. Mao, J. J. Gonzalez and R. E. Russo, *Appl. Phys. A: Mater. Sci. Process.*, 2013, 1–8.
19 X. Liu, S. Sun, X. Wang, Z. Liu, Q. Liu, P. Ding, Z. Guo and B. Hu, *Opt. Express*, 2013, **21**, A704–A713.
20 R. Le Harzic, D. Breitling, S. Sommer, C. Föhl, K. König, F. Dausinger and E. Audouard, *Appl. Phys. A: Mater. Sci. Process.*, 2005, **81**, 1121–1125.
21 T. Donnelly, J. Lunney, S. Amoruso, R. Bruzzese, X. Wang and X. Ni, *J. Appl. Phys.*, 2009, **106**, 013304.
22 A. Semerok and C. Dutouquet, *Thin Solid Films*, 2004, **453**, 501–505.
23 S. Amoruso, R. Bruzzese and X. Wang, *Appl. Phys. Lett.*, 2009, **95**, 251501.
24 S. Noël and J. Hermann, *Appl. Phys. Lett.*, 2009, **94**, 053120.
25 S. Noël, E. Axente and J. Hermann, *Appl. Surf. Sci.*, 2009, **255**, 9738–9741.
26 S. Amoruso, R. Bruzzese, X. Wang, G. O'Connell and J. Lunney, *J. Appl. Phys.*, 2010, **108**, 113302.
27 V. Piñon and D. Anglos, *Spectrochim. Acta, Part B*, 2009, **64**, 950–960.
28 V. Piñon, C. Fotakis, G. Nicolas and D. Anglos, *Spectrochim. Acta, Part B*, 2008, **63**, 1006–1010.
29 Z. Hu, S. Singha, Y. Liu and R. J. Gordon, *Appl. Phys. Lett.*, 2007, **90**, 131910.
30 S. Singha, Z. Hu and R. J. Gordon, *J. Appl. Phys.*, 2008, **104**, 113520.
31 X. Li, L. Jiang and H.-L. Tsai, *J. Appl. Phys.*, 2009, **106**, 064906.
32 L. Jiang and H.-L. Tsai, *Int. J. Heat Mass Transfer*, 2007, **50**, 3461–3470.
33 A. Chen, Y. Jiang, L. Sui, D. Ding, H. Liu and M. Jin, *Opt. Commun.*, 2011, **284**, 2192–2197.
34 H. S. Sim, S. Park, T.-H. Kim, Y. K. Choi, J. S. Lee and S. H. Lee, *Mater. Trans.*, 2010, **51**, 1156–1162.
35 J. Guo, T. Wang, J. Shao, T. Sun, R. Wang, A. Chen, Z. Hu, M. Jin and D. Ding, *Opt. Commun.*, 2012, **285**, 1895–1899.
36 S. Harilal, *J. Appl. Phys.*, 2007, **102**, 123306.

 This journal is © The Royal Society of Chemistry 2014

Published on 13 March 2014. Downloaded by Changchun Institute of Optics, Fine Mechanics and Physics, CAS on 26/03/2015 01:05:15.

37 S. Harilal, R. Coons, P. Hough and A. Hassanein, *Appl. Phys. Lett.*, 2009, **95**, 221501.
38 J. T. Schiffern, D. W. Doerr and D. R. Alexander, *Spectrochim. Acta, Part B*, 2007, **62**, 1412–1418.
39 Y. Lu, V. Zorba, X. Mao, R. Zheng and R. E. Russo, *J. Anal. At. Spectrom.*, 2013, **28**, 743–748.
40 A. Kasperczuk, T. Pisarczyk, M. Kalal, J. Ullschmied, E. Krousky, K. Masek, M. Pfeifer, K. Rohlena, J. Skala and P. Pisarczyk, *Appl. Phys. Lett.*, 2009, **94**, 081501.
41 M. A. de Araújo, R. Silva, E. de Lima, D. P. Pereira and P. C. de Oliveira, *Appl. Opt.*, 2009, **48**, 393–396.
42 S. Amoruso, C. Altucci, R. Bruzzese, C. De Lisio, N. Spinelli, R. Velotta, M. Vitiello and X. Wang, *Appl. Phys. A: Mater. Sci. Process.*, 2004, **79**, 1377–1380.
43 T. Y. Choi and C. P. Grigoropoulos, *J. Appl. Phys.*, 2002, **92**, 4918–4925.
44 A. De Giacomo, M. Dell'Aglio, D. Bruno, R. Gaudiuso and O. De Pascale, *Spectrochim. Acta, Part B*, 2008, **63**, 805–816.
45 A. De Giacomo, A. De Bonis, M. DellAglio, O. De Pascale, R. Gaudiuso, S. Orlando, A. Santagata, G. Senesi, F. Taccogna and R. Teghil, *J. Phys. Chem. C*, 2011, **115**, 5123–5130.
46 S. Beldjilali, W. Yip, J. Hermann, T. Baba-Hamed and A. Belasri, *Anal. Bioanal. Chem.*, 2011, **400**, 2173–2183.
47 C. Goueguel, S. Laville, F. Vidal, M. Sabsabi and M. Chaker, *J. Anal. At. Spectrom.*, 2010, **25**, 635–644.
48 A. Vorobyev and C. Guo, *Opt. Express*, 2006, **14**, 13113–13119.
49 X. Zhao and Y. C. Shin, *J. Phys. D: Appl. Phys.*, 2013, **46**, 335501.
50 M. Barberoglou, G. Tsibidis, D. Gray, E. Magoulakis, C. Fotakis, E. Stratakis and P. Loukakos, *Appl. Phys. A: Mater. Sci. Process.*, 2013, **113**, 273–283.
51 A. Chen, S. Li, S. Li, Y. Jiang, J. Shao, T. Wang, X. Huang, M. Jin and D. Ding, *Phys. Plasmas*, 2013, **20**, 103110.
52 L. Sudrie, A. Couairon, M. Franco, B. Lamouroux, B. Prade, S. Tzortzakis and A. Mysyrowicz, *Phys. Rev. Lett.*, 2002, **89**, 186601.
53 A. Couairon, L. Sudrie, M. Franco, B. Prade and A. Mysyrowicz, *Phys. Rev. B: Condens. Matter Mater. Phys.*, 2005, **71**, 125435.
54 P. Polynkin, B. Pasenhow, N. Driscoll, M. Scheller, E. M. Wright and J. V. Moloney, *Phys. Rev. A: At., Mol., Opt. Phys.*, 2012, **86**, 043410.
55 A. Couairon, *Phys. Rev. A: At., Mol., Opt. Phys.*, 2003, **68**, 015801.
56 P. Polynkin and J. V. Moloney, *Appl. Phys. Lett.*, 2011, **99**, 151103.
57 G. S. He, A. P. Zhang, Q. Zheng, H.-Y. Qin, P. N. Prasad, S. He and H. Agren, *Quantum Electron.*, 2009, **45**, 816–824.
58 A. Couairon and A. Mysyrowicz, *Phys. Rep.*, 2007, **441**, 47–189.
59 X. Li, W. Wei, J. Wu, S. Jia and A. Qiu, *J. Appl. Phys.*, 2013, **113**, 243304.
60 S. L. Chin, *Femtosecond laser filamentation*, Springer, 2010, vol. 55.
61 T. B. Petrova, H. Ladouceur and A. Baronavski, *Phys. Plasmas*, 2008, **15**, 053501.
62 A. Kumar, D. Dahiya and A. Sharma, *Phys. Plasmas*, 2011, **18**, 023102.
63 J. Papeer, D. Gordon, P. Sprangle, M. Botton and A. Zigler, *Appl. Phys. Lett.*, 2013, **103**, 244102.